To be submitted to IEEE J. Oceanic Engineering

Model-Data Assimilation of Internal Waves during ASIAEX-2001

Antony K. Liu, Yunhe Zhao
Oceans and Ice Branch, NASA Goddard Space Flight Center, Greenbelt MD, USA

T. Y. Tang
Institute of Oceanography, National Taiwan University, Taipei, Taiwan

Steven R. Ramp
Department of Oceanography, Naval Postgraduate School, Monterey CA, USA

Abstract -- In recent Asian Seas International Acoustics Experiment (ASIAEX), extensive moorings have been deployed around the continental shelf break area in the northeast of South China Sea in May 2001. Simultaneous RADARSAT SAR images have been collected during the field test to integrate with the in-situ measurements from moorings, ship-board sensors, and CTD casts. Besides it provides synoptic information, satellite imagery is very useful for tracking the internal waves, and locating surface fronts and mesoscale features. During ASIAEX in May 2001, many large internal waves were observed at the test area and were the major oceanic features for acoustic volume interaction. Based on the internal wave distribution maps compiled from satellite data, the wave crest can be as long as 200 km with amplitude of 100 m. Environmental parameters have been calculated based on extensive CTD casts data near the ASIAEX area. Nonlinear internal wave models have been applied to integrate and assimilate both SAR and mooring data. Using SAR data in deep water as an initial condition, numerical simulations produce the wave evolution on the continental shelf and compared reasonably well with the mooring measurements at the downstream station. The shoaling, turning, and dissipation of large internal waves on the shelf break, elevation solitons, and wave-wave interaction have been studied and are very important issues for acoustic propagation. The internal wave effects on acoustic modal coupling has been implicated and discussed.

Index Terms – Remote sensing, internal waves, shallow water.

I. INTRODUCTION

The ocean current over topographic features such as a sill or continental shelf in a stratified flow can produce nonlinear internal waves of tidal frequency and has been studied by many researchers [1], [2], [3]. Their observations provide insight into the internal wave generation process and explain the role they play in the transfer of energy from tide to ocean mixing. It has been demonstrated that surface signatures of these nonlinear internal waves are observable in the Synthetic Aperture Radar (SAR) images [4] from Russian Almaz-1 and from the First and Second European Remote sensing Satellite ERS-1/2 [5]. Recently, the internal wave distribution maps in the northeast of

South China Sea (SCS) and near Hainan Island have been compiled from hundreds of ERS-1/2, RADARSAT and Space Shuttle SAR images from 1993 to 1998 by [6]. Based on internal wave distribution map, most of internal waves in the northeast part of South China Sea are propagating westward. The wave crest can be as long as 200 km with amplitude of 100 m, due to strong current from the Kuroshio branching out into the South China Sea [7]. From the observations at drilling rigs near DongSha Island by Amoco Production Co. [8], the solitons may be generated in a 4 km wide channel between Batan and Sabtang islands in Luzon Strait. However, recent work [7], [9] has suggested that solitons in SCS may also be generated locally near the shelf break. Furthermore, based on satellite imagery the long crest internal waves near Luzon Strait are produced by the connection along the crest of many individual wave packets generated from different sources or sills in the strait [7].

The essential element of the surface effects is the interaction between the internal wave-induced surface current field and the wind-driven ocean surface waves. For a linear SAR system, the variation of the SAR image intensity is proportional to the gradient of the surface velocity, or to the strain rate. The proportionality depends on radar wavelength, radar incidence angle, angle between the radar look direction and the internal wave propagation direction, azimuth angle, and the wind velocity [4]. For the high wind speed condition, the internal wave signal maybe too weak to be observed by radar due to low signal-to-noise ratio. When the internal waves propagate in the cross-wind direction, the wave-current interaction is also relatively weak, and so is the radar backscattering for SAR observation. The strain rates have been calculated for the internal wave packets and their values are consistent with the observed data from New York Bight internal waves [3]. Without in-situ field measurements for detailed numerical simulations, the comparison of relative modulation from SAR data and strain rate from model are reasonable qualitatively [7].

It has been demonstrated that internal waves are responsible for the anomalous frequency response of shallow-water sound propagation [10]. They found that acoustic transmission loss is sensitive to the signal frequency and is a "resonance-like" function of the soliton wavelength and packet length. This resonant coupling effect is caused by strong horizontal gradient in sound speed induced by internal solitons. An overview of the 1995 SWARM shallow-water internal wave acoustic scattering experiment is reported by investigators [11]. Both comparison with acoustic model simulations and correlation with physical measurements point to solitons in the wave-guide as the major source of mode-coupling during the SWARM experiment [12]. Based on acoustic model analysis, acoustic impact is strongly affected by the internal wave parameters: soliton number, location, direction, and wavelength. Furthermore, more soliton activity is closer to receiver, the greater the spreading and bias result in acoustical signal arrivals.

Since 1997, U.S. and Asian Pacific Rim scientists have initiated a joint effort to design and conduct an experiment to study shallow-water acoustics, physical oceanography, and bottom structure in the South and East China Seas. This experiment has been named the Asia seas International Acoustics Experiment (ASIAEX). A series of pre-tests in SCS for area survey started from 1999 [13], in conjunction with modeling and remote sensing

studies. In recent South China Sea internal wave study, as a part of the ASIAEX pre-test program, five moorings had been deployed in April 2000 for a month. Simultaneous SAR coverage from ERS-2 and RADARSAT had been collected and processed from Taiwan ground station in near real-time [14]. This preliminary survey from year 2000 definitely helped on the planning for the major field experiment in May 2001. In this paper, the research work on the internal wave study is focused especially on modeling and remote sensing efforts to support the ASIAEX-2001.

ASIAEX-2001 in SCS has focused on acoustics volume interaction, and used three ships (R/V OR-1, OR-3, and Fisheries Researcher-1) from Taiwan [15]. The mooring deployments had been done by the end of April [16], and SEASOAR surveys was carried out from April 29 to May 14 [17]. The intensive period of measurements was from May 3 to May 18. During the field test, a typhoon (Cimaron) was passing through ASIAEX area around May 12. Mooring recovery started after May 18 to 24. Based on the observations from SAR, SEASOAR and mooring data, the internal wave field was dominant in the ASIAEX area and its magnitudes were also larger than predicted from the planning. In this paper, SAR and in-situ observations during ASIAEX-2001 used in this study are first described. Next, SAR and mooring data analysis are presented in the following sections with the comparison of SAR and mooring data for internal wave parameters. Then, the evolution model of nonlinear internal waves on shelf is formulated and numerical simulations are performed for comparison. Finally, the internal wave characteristics near the ASIAEX area are summarized and their effect and impact on acoustic volume scattering is discussed.

II. OBSERVATIONS DURING ASIAEX-2001

Besides it provides synoptic information, satellite remote sensing is critical to several aspects of ASIAEX, including tracking the internal waves, and locating surface fronts and mesoscale features. On January 25, 2001 ERS-2's gyro#1 failed. ESA continues ERS-2 operations using the extra-backup-mode, which is a coarse attitude control mode as the first step of the gyro-less operations mode. So, the quality of ERS-2 SAR is highly degraded and Taiwan ground station can no longer process SAR images. In replacement, all cloud-free SPOT images (60km * 60km) with 20m resolution were collected and processed in near-real time during ASIAEX from Taiwan ground station. However, most of days during ASIAEX, the SPOT images were obscured by the cloud-cover and internal waves were visible only on May 7 and May 14, 2001.

Four RADARSAT ScanSAR images (500km * 500km with 100m resolution) from May 2, May 9, May 18, and May 11 2001 were ordered and collected during ASIAEX through RADARSAT International. On May 11, the SAR data were lost due to transmission problem, so an image from June 4 was provided instead. Figure 1 shows the schematic diagram of internal wave distribution map in the ASIAEX area delineated from RADARSAT ScanSAR images collected in May 2001. ScanSAR data coverage areas are shown by three large overlapped square boxes for May 2, 9, and 18. The small square box indicates the ASIAEX test area. As an example, Figure 2 shows the RADARSAT

ScanSAR image collected northeast of the South China Sea on May 9, 2001. Large internal wave packets in the ASIAEX area and squall lines with rain cells (bright areas) can be clearly identified. More RADARSAT standard high-resolution SAR images (100*100 km) from April 17, 18, 24 and May 1, 4, 5, 19, 26, 28 have been collected during ASIAEX through Naval Research Laboratory (NRL) and processed/archived at National Oceanic and Atmospheric Administration (NOAA) Satellite Active Archive (SAA).

The experiment setup has been reported by [15] in ASIAEX overview. Six moorings along the west-side of ASIAEX box is shown in a locator map with bottom topography [16]. As an example, mooring data from S7 located at 21° 36.9'N, and 117° 17.0'E has been processed [16] and Figure 3 shows two-hour high-pass filtered temperature data from mooring S7 from 16:00 May 9 to 04:00 May 10, 2001. The solitons measured near 22:00 at S7 (indicated by a white star in Figure 2) on May 9 corresponds to the solitons observed in SAR image (collected at 21:57:34). Based on ADCP measurement this is a mode-1 internal wave signal with the solitons moving WNW in the upper layer and ESE in the lower layer. The crossover point is near 150 m in a depth of 350m water. The wave-induced velocities exceed 120 cm/s in the upper layer and 100 cm/s in the lower layer. Based on temperature data, the soliton-induced fluctuation can be as large as 8° C with amplitude of 75 m. This packet looks only vaguely rank-ordered, with most of the energy in the dominant central spike.

CTD casts data have been collected extensively in April and May around ASIAEX area [18]. Figure 4 shows the location of CTD stations during ASIAEX-2001 in the South China Sea. S1 to S7 and LOCOs [19] are near oceanographic moorings, and 01, 02, 08, and 18 are near acoustic moorings. CTD data were also collected from S8, 2, 3, 4, and KA1 in deep water. The range of water depth for CTD data covers from 70 m to 2000 m. During ASIAEX-2001, many marine radar images from R/V OR-1 have been recorded from May 3 to May 10. The ship track was focused on the shelf break area in shallow water with a serpentine pattern for internal wave evolution. These marine radar, EK500 echo sounder, ship-board ADCP, and SEASOAR data [17] can be very useful to combine with SAR and mooring data for internal wave evolution study in the shelf break area. These data sets have been compiled with special focus on internal wave case study in May [20].

III. SAR DATA ANALYSIS

In this paper, the nonlinear internal waves have been studied with focus only on their evolution near the ASIAEX areas to complement with the acoustic application. As shown in Figure 1, two large internal wave packets in the ASIAEX area can be easily identified on May 9, and the internal waves are dominant features in the ASIAEX area in May 2001. Figure 2 shows internal wave packets (AB and CD), moorings S5, S7, S8 in white stars, and squall line with rain cells as very bright areas along the front. Based on the separation distance between packets, and semi-diurnal tidal theory, the wave speed and direction in deep basin can be estimated to be 1.7 m/s and 298 degree from north.

Transects across and perpendicular to the wave fronts of packets are shown in Figure 5(a) A1-B1, (b) A2-B2, (c) AB, (d) A3-B3, (e) A4-B4, and (f) A5-B5 showing the variability of solitons along the wave front of the second packet in Figure 2. Notice that the variation of the SAR image intensity/grayscale is proportional to the gradient of the surface velocity, which is to the ratio of amplitude by soliton width. So, the largest soliton in SAR image does not necessary correspond to the largest soliton in the mooring data. This second packet AB does not look rank-ordered, and it passed mooring S8 then arrived at moorings S7 and S5 on May 10. Notice that the soliton locations and amplitudes along wave front (A1-B1 to A5-B5) are quite different and imply the two-dimensional property of these solitons especially in shallow water. Due to the variation of these solitons along the wave front, the mooring measurements at downstream will be also quite different since each mooring observation is coming from different upstream transects. Notice that the mooring line from S2 to S7 is not lined up in the internal wave propagation direction as shown in SAR image (Figure 2).

Based on this radar backscatter data, three solitons have been observed in the second wave packet AB, and their wavelengths (or separation distances) of 3.2 km and 2.0 km are estimated as summarized in Table 1. The water depth of each mooring station is presented for reference. Local wave speed near mooring stations can be estimated based on the distance and time separation between solitons at mooring and in SAR observations, respectively. For example, the wave speed of 1.54 m/s can be estimated based on the distance (4.2 km) and time (45 min) between solitons observed at S7 and in SAR image, respectively. Similar procedure has been applied to the mooring S8 and SAR image, and the resultant internal wave speeds are shown in Table 1 as in parentheses. The number of solitons in each packet and the separation distance between solitons (wavelength) can be also estimated from mooring measurements once the local wave speed is known. The soliton widths in two packets can be estimated to be 1.4 and 2.5 km from KdV type model as discussed by [21] using SAR data such as the transects shown in Figure 3.

In order to validate these SAR observations with in-situ sea truth, internal wave evolution on May 4-5, along with May 9-10, has also been focused as the case study in this paper. Figure 6 is a RADARSAT Standard SAR image collected over ASIAEX area on May 5, 2001, showing internal wave packets (EF) and mooring S4, S5, S6, and S7 by stars. Figure 7 shows (a) SAR transect across and perpendicular to soliton packet along E1-F1 compared with (b) ADCP current data at mooring S5 on May 5 for reference. Local wave speed near mooring stations can also be estimated based on the distance and time separation between mooring and SAR observations. For example, the wave speed of 1.10 m/s can be estimated based on the distance (4.53 km) and time (69 min) between S5 and wave front in SAR image. Similar procedure for wave speed has been applied to the SAR and mooring data at S5, S6, S7 on May 4, and S4, S5, S6, S7 on May 5 as in parentheses (Table 2), respectively. The internal wave parameters from these two wave packets on May 4-5 are summarized in Table 2.

However, the internal wave field in ASIAEX area sometimes can be quite complicated. As shown in Figure 8 on May 18, besides the regular soliton packet propagating in the west direction, there are the second wave packets refracted and generated by Dongsha

Island propagating to the north in ASIAEX area. These two wave systems, an east-west propagating soliton system from the Luzon Strait and another local generated north-south linear wave packet from shelf break, have been merged as a circle by the nonlinear wave-wave interaction. The intersection areas show an interrupted front with a kink as a result of wave interaction. Figure 9 show three zoomed-in subscenes (12.8 km in size) of SAR images and wave spectra from (a) east-west soliton system, (b) north-south linear wave, and (c) merged wave packet, respectively. The solitons have an averaged wavelength/separation of 1.2 km and the wavelength of linear waves is about 900 m, while the merged wave packet has a wavelength of 750 m only with a north-west propagation direction. This nonlinear wave-wave interaction is quite similar to the observation in the Yellow Sea [6]. Not only has the direction of wave train shifted after interaction, but the number of waves in the wave packet and their wave amplitudes has also changed. The similar wave-wave interaction pattern has also been observed on May 4, two weeks before, which maybe related to the tide cycle. Two wave systems can be easily identified, but the interaction is not as strong as on May 18 due to weak soliton energy in tidal cycle. The two-dimensional wave pattern of this two-wave field is crucial for the interpretation of acoustic measurement which may cause acoustic horizontal refraction in additional to mode-coupling [22].

IV. MOORING DATA ANALYSIS

Mooring data from S2, S4, S5, S6, S7, and S8 are used for this internal wave study. The water depths of each mooring and the separation distances between them are summarized in Table 1. There are two wave packets AB and CD as shown in SAR image on May 9. First the soliton packets are identified from ADCP data based on SAR image (Figure 2), so the shift/lagging time between moorings can be estimated from the arriving time of each identified packet. For example, Figure 10 shows ADCP current time series data from moorings S5, S6, and S7 at different depths of 157m, 100m, and 55m respectively with soliton packets identified from SAR image (Figure 2) on May 9 to 10, 2001 showing mode-1 internal waves passing through ASIAEX area. The modal structure in the vertical can also be shown in more detailed plot [16]. Then ADCP velocity components have been re-combined or rotated to find the direction of maximum current induced by internal waves; that is the internal wave propagation direction. The mooring horizontal line is about 286 degree from the North. So, the shift distances between moorings along wave propagation direction can be calculated as listed in Table 1.

Using the shift distance and time along wave propagation direction, the internal wave speed between moorings for each packet has been computed to compare with SAR data result. In deep water, wave speed of 1.7 m/s agrees well with estimate of 1.77 m/s near S8. On the shelf in ASIAEX area, the wave speeds (in m/s) are slowing down quickly from 1.77 and 1.57 (at S7/S8) to 1.14 (at S6/S7), 1.08 and 1.26 (at S5/S6), 0.76 and 0.77 (at S4/S5), 0.72 (at S2/S4) for packets CD and AB respectively. Also, waves are shifting direction from 25 degree from the West to 25, 45, 45, 75 degree. Local wave speeds near mooring stations have also been estimated based on SAR and mooring observations (Figure 2) as discussed before. These speeds of 1.67 m/s at S8, and 1.54 m/s at S7 as

shown in parentheses (Table1) are quite consistent with the results of mooring data. Notice that the linear wave speeds at various depths will be calculated from dispersion relation using CTD data of density profiles.

In addition, number of solitons in packets, soliton widths, and wavelengths can be estimated based on KdV type model. Three solitons in packets are identified at S5, S6, and S7 as also observed from SAR data. For wave packet CD, the soliton widths are found to be 0.7 km at S4, 1.5 km at S5, 0.9 km at S6, and 1.4 km at S7 which is consistent with SAR observation of 1.4 km. The separation distances (or wavelengths) are 2.4-1.6 km at S5, 4.2-1.6 km at S6, 4.4-2.1 km at S7, and 9.7-2.4 km at S8. The SAR estimates of separation distances are 4.3-2.8 km that is also consistent with observations at S6 and S7. Similar consistent results have also been obtained for wave packet AB as shown in Table 1. The current induced by internal waves can be obtained from ADCP data, and it ranges from 0.5 to 1.2 m/s for CD packet and 0.4 to 1.6 m/s for AB packet. Once, the current profile induced by wave is determined from ADCP data, the wave amplitude will be estimated from the internal wave model. A comparison of SAR and mooring data for internal wave field on May 9-10, 2001 is summarized in Table 1. The comparison of internal wave speed, direction, width, length, and amplitude derived from ADCP data at moorings (S2 – S8) and SAR data in ASIAEX region show good agreement and consistent results on May 9, 2001.

In order to show the variability of typical wave characteristics estimated from May 9-10, the exactly same procedure of data analysis has been followed for May 4-5 SAR and mooring data. Similar results of internal wave field on May 4-5, 2001 are also summarized in Table 2. Due to the wave-wave interaction near S5 on May 4, the wave direction and speed are confused as discussed before (indicated by stars). In general, there were two wave systems, an east-west propagating soliton system from the Luzon Strait and another local generated north-south linear wave packet from shelf break near Dongsha Island, merged by the nonlinear wave-wave interaction. On May 4 (packet GH), there is a linear wave train with wavelength of 200 m, speed of 0.75-1.2 m/s (S4 to S6), and is mostly propagating northward. On May 5 (packet EF), the wave packet consists solitons generated from Luzon Strait and is mostly propagating westward.

For example in packet EF, the wave speed (in m/s) is found to be 1.16 between S5/S6, 1.32 between S6/S7, and 1.47 between S7/S8 as compared with SAR estimate of 1.26 m/s on shelf (Figure 6). Number of solitons in packets varies from 1 to 3 as the wave evolved on shelf. Soliton width of 0.8 to 1.2 km is narrow as compared with SAR observation of 1.5 km. The separation distances (or wavelengths) are 1.3 to 1.0 km at S4, 2.1 km at S5 and 1.9 to 1.5 km at S6 that is consistent with SAR observation of 2.0 km. The current induced by internal waves can be obtained from ADCP data, and it ranges from 0.5 to 0.7 m/s for EF packet and 0.3 for GH packet. Based on the currents estimated from ADCP, the wave amplitudes on May 4-5 are estimated to be only the half of that from May 9-10. The small waves on May 5 as compared with twice larger waves on May 10 are because of weak soliton energy in tidal cycle; the strongest solitons are generated around spring tide on May 8 and 9 [16].

V. NONLINEAR INTERNAL WAVE EVOLUTION ON A SHELF

The evolution of nonlinear internal wave packet on a continental shelf has been studied and formulated [3], [7]. The dissipation effects on solitary wave evolution are considered to be important in the shallow water owing to internal wave breaking and strong turbulent mixing. The evolution equation of nonlinear internal waves in water of depth H(x,t) and amplitude A(x,t) with variable coefficients is given by

$$A_t + C_o A_x + \alpha A A_x + \gamma C_o A_{xxx} - \varepsilon A_{xx} = 0 \qquad (1)$$

where C_0 is the linear wave speed for very long waves (k→ 0), and the wave-induced velocity is

$$U(z) = C_o A_o \phi'(z) \qquad (2)$$

The eigenvalue problem for the vertical modes is

$$\phi'' + [N^2 - \omega^2]\phi / C_o = 0, \quad \phi(0) = \phi(-H) = 0, \quad C_o = \omega / \kappa \qquad (3)$$

Where ω and κ and are wave frequency and wavenumber, and $|\phi|_{max}$ =1. N(z) is the Brunt-Vaisala frequency or stability frequency.

The environmental parameters for the nonlinear term is

$$\alpha = 3C_o \int_{-H}^{0} \phi'^3 dz \Big/ 2\int_{-H}^{0} \phi'^2 dz \qquad (4)$$

and for the dispersion term is

$$\gamma = \int_{-H}^{0} \phi^2 dz \Big/ 2\int_{-H}^{0} \phi'^2 dz \qquad (5)$$

and ε is the eddy viscosity for the dissipation term.

An effective horizontal eddy viscosity of ε = 1 to 10 m^2/s for solitons was used [2], [3]. Because eddy viscosity is not a property of a fluid, its value may vary with location and water depth. It is possible that local, incipient shear flow instability or wave breaking could be a cause leading to an eddy viscosity of such value. For shallow water in the ASIAEX area, the bottom friction and induced mixing can be another dissipation mechanism.

Density profiles are provided from CTD casts data collected during ASIAEX [16]. As an example, Figure 11a, and 11b show the density and B-V frequency profiles of CTD cast on April 20, 2001 at S6 mooring. The peak of B-V frequency profile is at 50 m

approximately. The vertical mode-1 eigenfunction and its derivative are shown in Figure 12a, and 12b. Notice that the peak of mode-1 eigenfunction is at 100 m which is approximately the base of the main thermocline. The linear wave speed is determined by the eigenvalue and is found to be $C_0 = 1.06$ m/s for mode-1 wave ($\kappa = 0.0001$ m^{-1}). From Equation 2, then the wave amplitude can be estimated based on ADCP current measurements of solitons. Figure 12b shows the best fit of ADCP current measurements in packet AB (as triangles) and CD (as circles) to mode-1 eigenfunction derivative and results in the wave amplitude A_0 of 63 m and 32 m respectively. The same procedure has also applied to mooring S7 and S5 and results in the wave amplitudes of 70/95 m and 80/90 m respectively.

In order to demonstrate the effects of varying depth on the environmental parameters, all CTD casts data collected extensively in April and May around ASIAEX area are used to solve the eigenvalue problem (Equation 3) for various depths. Figure 13a shows the resultant environmental parameters α and γ as a function of depths. Notice that the nonlinear parameter α is across zero at depth of 100 m and peaked at 300 m approximately. The linear wave speed C_o and wave speed C as a function of depths is shown in Figure 13b where wave speed data is collected from Table 1 and 2. The difference between C and C_o is mostly because of the nonlinear effects. These results for a wave propagating from a deep water of 800 m near the edge of the continental shelf to a nearshore water depth of 70 m can be summarized as follows: (1) the wave speed is reduced to less than half of its initial value, which shows wave speed retardation due to shoaling in shallow water; (2) the parameter γ for the dispersive effect decreases exponentially, which indicates the compression of the wave; (3) the parameter α for the nonlinear effect is relatively flat in deepwater, then peaks up at 300 m depth, decreases rapidly in shallow water, and it is across a location of critical depth of 100 m where $\alpha = 0$. Because α changes sign, the wave of depression will not survive after critical location and may disintegrate into a dispersive wave train, then evolve into an elevation packet [7].

In general, the main body of the stratification could not change much in a few weeks, but the stratification in the upper 80 m could certainly change due to meteorological forcing and seasonal variation. As observed from the CTD data, the mixed layer depth is about 45 m at depth of 100 m, and it is thickening to about 60 m at the depth of 270 m to shelf break and in deep water during ASIAEX-2001. The peak observed in nonlinear parameter α at depth 270 m in Figure 13 is probably caused by this variation of mixed layer depth. Elevation waves have also been observed in mooring data at 120 m depth [16]. Therefore, the critical depth is not a static parameter, but depends on how the mesoscale current, internal tidal bore, and the waves themselves impact the thermocline depth.

VI. NUMERICAL SIMULATION AND COMPARISON

The evolution of nonlinear internal waves is based upon the balance of nonlinear effects with the dispersive effects. This evolution can be simulated numerically by solving the Kortweg-deVries type equation (1) with varying coefficients corresponding to the changing environment as demonstrated before [2], [3], [7]. The dissipation effects on nonlinear wave evolution are important in the shallow water owing to internal wave breaking and strong turbulent mixing. The effects of varying depth on the numerical simulation of nonlinear wave evolution can be considered to fall into two categories: (1) The appearance of variable coefficients in the K-dV type evolution equation represents the first-order effect; (2) the shoaling effects due to variation of wave speed/eigenfunction along the path of wave propagation; (3) the dissipation effects vary with location and water depth. Near ASIAEX area approaching shelf break, the wave amplitude initially will increase significantly due to shoaling effects. Once the solitons become highly nonlinear on shelf break, the eddy viscosity may increase and could be eroding the sharp peaks of the large solitons, reducing their amplitudes and increasing their apparent widths at the same time. Therefore the shoaling effect eventually could be suppressed by the dissipation effect.

A numerical approach using Fornberg's pseudo-spectral method [2], [3], [7] has been developed to solve the evolution Equation (1). A Fast-Fourier Transform (FFT) algorithm is used in the spatial coordinate and the split-step method is used for time derivatives. The choice of time step and mesh size has to be made with care in order to obtain an accurate numerical solution. The time step was chosen in order to maintain numerical stability; the computational reference frame was chosen to move in the direction of wave propagation at a certain constant speed such that the wave train remains in the computational domain. Thus, changes in wave speed as well as shape will become apparent in a space-time evolution plot. Also, the Hanning window is used to filter out any waves entering the computational domain from the adjacent domain.

A numerical simulation is performed by solving the initial value problem described by Equation (1) with SAR observation of a soliton near S8 on May 9, 2001 as an initial condition. The initial condition of a well-developed soliton in deep water (about depth of 1 km) is given by

$$A = A_o \, \mathrm{sech}^2 (x / L) \qquad (6)$$

where A_o = 80 m, L = 1.5 km which corresponds to a width of 3 km, are used.

Figure 14a shows the simulated space-time evolution of nonlinear internal waves in the ASIAEX area from deep water (1 km) to S5 (180 m) with variable environmental parameters and dissipation effects. Because eddy viscosity is not a property of a fluid, its value may vary with location and water depth. For this case study, the effective horizontal eddy viscosity $\varepsilon = 1$ m^2/s in deep water linearly increased to 6 m^2/s in shallow water at S5 is used. In this sequence, an initial well-developed soliton in deep water develops to a large wave packet due to bottom effect. The wave amplitude initially will increase significantly and its width decrease at the same time due to shoaling effects. The simulation window is moving with a reference speed of 1.5 m/s. Once the solitons

become highly nonlinear on shelf break, the eddy viscosity increase and erode the sharp peak of the large soliton, reducing its amplitudes. Near S5 in shallow water it evolves into a large wave packet of three rank-ordered solitons after 12 hours.

The numerical simulated wave amplitudes are 60, 40, and 30 m with peak-to-peak distances of 7.1, and 1.3 km. As compared with mooring data at S5 in Figure 14b, the wave amplitudes are 80, 40, and 32 m with peak-to-peak distances of 7.6, and 1.8 km. Therefore, from a SAR observed initial soliton at upstream, the numerical simulation compares reasonably well with the measurements at the distant mooring S5 for three solitons in a large wave packet as regards their amplitudes and wavelengths and wave speeds. This type of numerical simulation demonstrates the method of data assimilation to integrate all data from SAR, moorings, CTD casts, and ship-board marine radar. The data assimilated results, then, can be used as inputs for acoustic volume scattering simulation to compare with acoustics data in SCS.

Figure 15a shows the numerical evolution of the internal soliton packet propagating from mooring S5 (Figure 14a) to mooring S3 (depth of 85 m) in shallow water with a decreasing dissipation from $\varepsilon = 6$ m^2/s to 2 m^2/s linearly. The change of polarization from depression waves to elevation waves across the critical depth has been demonstrated in this simulation. Since the nonlinear parameter is across zero at a location of critical depth of 100 m, the waves of depression can not survive after critical location (about 2.5 hr) and may disintegrate into a dispersive wave train (after 4 hr), then evolve into an elevation wave packet (after 6.25 hr). The linear decreasing dissipation (but still large than 2 m^2/s) can be caused by less shoaling and breaking effects with less depth change along the wave propagation path in shallow water on the shelf. In order to demonstrate the effect of the coefficient of dissipation on wave packet evolution, the dissipation parameter $\varepsilon = 6$ m^2/s is hold to be constant for the next calculation as shown in Figure 15b. Notice that in this case of constant dissipation the soliton does not change the polarization completely from depression waves to elevation waves across the critical depth as demonstrated in the first simulation. Because of relatively larger dissipation in shallow water (within 100 m), the sharp peaks of elevation have been eroded and damped by the dissipation. This second simulation is also consistent with the observations from the shallow moorings [19]. Since eddy viscosity may vary with location and water depth, therefore, the change of polarization from depression waves to elevation waves across the critical depth is always possible as observed before when the environment condition along the wave propagation path is favorable [23].

VII. SUMMARY AND DISCUSSION

In this paper, nonlinear internal wave evolution in the northeast of South China Sea is studies based on the ASIAEX SAR, CTD, and mooring data. The collection of SAR images in conjunction with the moorings and field measurements in the South China Sea is not only crucial to provide synoptic map of internal wave field but also important to identify and track each individual soliton packet encountered at moorings. Selective sets of mooring data concurrent with SAR observations are presented and analyzed for the

parametric study of internal wave characteristics. Based on the results from SAR and mooring data in Table 1, the environmental condition and typical internal wave characteristics near the ASIAEX area on May 10, 2001 can be summarized as follows: a) water depth is from 800 m near shelf break to 70 m in shallow water; b) internal wave direction is shifting from 295° to 345°; c) internal wave speed ranges from 1.8 m/s to 0.72 m/s; d) soliton width is approximately from 1.7 km to 0.7 km; e) soliton number in packet is from 5 to 3 to wave train in shallow water; f) soliton separation ranges from 9.7 km and 2.4 km to wavelength of 1.2 km; g) wave amplitude in average is from 95 m to 63 m and less in shallow water. As mentioned before, acoustic impact is strongly affected by these internal wave parameters. Furthermore, these observations have provided a calibration on SAR data and inputs for the numerical simulation of nonlinear wave evolution on the continental shelf.

The mesoscale variability, mean horizontal and vertical shears and varying stratification near the shelf-break are highly transient in April/May during the spring transition from winter monsoon to summer typhoon season. Therefore, the evolution of internal solitons in the ASIAEX test area at shelf-break is especially complicated in April/May with many interested features such as mode-two solitons [14]. The solitons are in transient with continuous evolution and dissipation along the shelf. During ASIAEX, nonlinear internal waves propagating up the slope have been tracked by research ship as reported by [23]. The location of the initiation of the depression to elevation conversion has been identified in their high-resolution acoustic data.

It is clear that these internal wave observations near the ASIAEX area provide a unique resource for addressing a wide range of processes on soliton propagating up the slope. Among these the following are included: 1) the disintegration of solitons into internal wave packets, breaking, and dissipation; 2) the shoaling effects of variable bottom topography on wave evolution, generation of mode-two waves, and internal wave-wave interaction; 3) the evolution of nonlinear depression waves through the critical depth to convert to elevation waves. Numerical simulations have been performed by using SAR observed internal wave field in the shelf break region as an initial condition to produce the wave evolution. The numerical simulation compares reasonably well with the measurements at the downstream mooring S5 on shelf for three solitons in a large wave packet as regards their amplitudes and wavelengths and wave speeds. This type of numerical simulation demonstrates the method of data assimilation to integrate all data from SAR, moorings, CTD casts, and ship-board marine radar. The inclusion of these physical processes is essential to improve quantitative understanding of the coastal dynamics and the sensitivity for acoustic propagation.

The data assimilated results, then, can be used as inputs for acoustic volume scattering simulation to compare with acoustics data in SCS. Based on acoustic modal coupling analysis [10], significant energy transfer will occur between acoustic modes m and n if $k_{int} = k_n - k_m$, where k_{int} is the wave number of the internal wave. Since the wavelength of internal waves is several km, the internal wave number k_{int} is very small compared with acoustic wave numbers k_n and k_m. Effective k_{int} is even smaller when the wave evolution path is not aligned with acoustic source and receiver. Therefore, only neighboring

acoustic high-modes are sensitive to coupling events initially as reported by [24]. But, acoustic modal coupling will eventually trigger-down to the low modes due to the complicate three-dimensional internal wave pattern. In general, attenuation is greater for higher acoustic modes. Differences in acoustic modal group velocities cause time spreading of pulses. So, higher modes act as energy sink and cause significant variability in apparent attenuation and arrival-time for low modes. As an inverse problem, low-frequency acoustic measurements from two receivers in different directions could be a potential tool for remote sensing of internal wave activity in the coastal zone. Further acoustic volume scattering study based on the assimilated internal wave field is underway and will be report in the near future.

ACKNOWLEDGMENT

The authors wish to thank ASIAEX science team for their valuable discussions and suggestions, especially to M.-K. Hsu of the National Taiwan Ocean University, and J. Wang of the National Taiwan University. Help provided by Y.-J. Yang of the Taiwan Navy Academy to collect mooring data is also acknowledged. The RADARSAT SAR images are collected under special project and from NOAA Satellite Active Archive (SAA), and all SAR data are copyrighted by Canada Space Agency (CSA). ASIAEX work has been supported by U.S. Office of Naval Research (ONR) and also funded by Taiwan's National Science Council (Tang).

REFERENCES

[1] J. R. Apel, J. R. Holbrook, A. K. Liu, and J. Tsai, "The Sulu Sea internal soliton experiment," *J. Phys. Oceanogr.*, vol. 15, pp. 1625-1651, 1985.
[2] A. K. Liu, J. R. Apel, and J. R. Holbrook, "Nonlinear internal wave evolution in the Sulu Sea," *J. Phys. Oceanogr.*, Vol. 15, pp. 1613-1624, 1985.
[3] A. K. Liu, "Analysis of nonlinear internal waves in the New York Bight," *J. Geophys. Res.* Vol. 93, pp. 12317-12329, 1988.
[4] A. K. Liu, and S. Y. Wu, "Satellite remote sensing: SAR," *Encyclopedia of Ocean Sciences*, London: Academic Press, Edited by J. H. Steele, S. A. Thorpe, and K.K Turekian, vol. 5, pp. 2563-2573, 2001.
[5] N. K. Liang, A. K. Liu, and C. Y. Peng, "A preliminary study of SAR imagery on Taiwan coastal water," *Acta Oceanogr. Taiwanica.*, vol. 34, pp. 17-28, 1995.
[6] M. K. Hsu, A. K. Liu and C. Liu, "A study of internal waves in the China Seas and Yellow Sea using SAR," *Continental Shelf Res.*, vol. 20, pp. 389-410, 2000.
[7] A. K. Liu, Y. S. Chang, M. K. Hsu and N. K. Liang, "Evolution of nonlinear internal waves in the East and South China Seas," *J. Geophys. Res.* Vol. 103, pp. 7995-8008, 1998.
[8] J. B. Bole, C. C. Ebbesmeyer, and R. D. Romea, "Soliton currents in the South China Sea: measurements and theoretical modeling," Offshore Technology Conference, OTC 7417, 367-376, 1994.
[9] M. K. Hsu, and A. K. Liu, "Nonlinear internal waves in the South China Sea," *Canadian J. Rem. Sens.*, vol. 26, pp. 72-81, 2000.
[10] J.-X. Zhou, X.-Z Zhang, and P. H. Rogers, "Resonant interaction of sound wave with internal solitons in the coastal zone," *J. Acost. Soc. Am.*, vol. 90 (4), Pt. 1, pp. 2042-2054, 1991.
[11] J. R. Apel, M. Badiey, C.-S. Chiu, S. Finette, R. H. Headrick, J. Kemp, J. F. Lynch, A. Newhall, M. H. Orr, B. H. Pasewark, D. Tielbuerger, A. Turgut, K. Heydt, S. Wolf, "An overview of the 1995 SWARM

shallow-water internal wave acoustic scattering experiment," *IEEE J. Oceanic Eng.*, vol. 22, pp. 465-500, July 1997.
[12] R. H. Headrick, "Analysis of internal wave induced mode coupling effects on the 1995 SWARM experiment acoustic transmissions," Ph.D. dissertation. MIT/WHOI Joint Program in Oceanography and Ocean Engineering, pp. 195, 1997.
[13] Y.-J. Yang, et al., this issue, 2004.
[14] A. K. Liu, and M. K. Hsu, "Nonlinear internal wave study in the South China Sea Using SAR," *Int. J. Remote Sens.*, in press, 2003.
[15] J. F. Lynch,et al., this issue, 2004.
[16] S. R. Ramp, D. Y. Tang, T. Duda, J. F. Lynch, A. K. Liu, C.-S. Chiu, F. Bahr, H.-R. Kim, and Y. J. Yang, this issue, 2004.
[17] G. Gawarkiewicz, et al., this issue, 2004.
[18] T. Y. Tang, et al., this issue, 2004.
[19] T. Duda, et al., this issue, 2004.
[20] T.-Y. Lin, "Characteristics of nonlinear internal waves in the north of South China Sea," Master dissertation. Inst. Oceanography/NTU, pp. 60, 2001
[21] Q. Zheng, Y. Yuan, V. Klemas, and X.-H. Yan, "Theoretical expression for an ocean internal soliton synthetic aperture radar image and determination of the soliton characteristic half width," *J. Geophys. Res.*, vol. 106, pp. 31415-31423, 2001.
[22] C. F. Chen, et al., this issue, 2004.
[23] M. H. Orr, and P. C. Mignerey, "Nonlinear internal waves in the South China Sea: Observation of conversion of depression internal waves to elevation internal waves," *J. Geophys. Res.*, Vol. 108, No. C3, 3064, doi:10.1029/2001JC001163, 2003.
[24] C.-S. Chiu, et al., this issue, 2004.

Table 1. SAR AND MOORING DATA COMPARISON on May 9-10

SENSOR (ADCP)	S2	S4	S5	S6	S7	S8	SAR
DEPTH (m)	71	120	184	275	350	800	---
DISTANCE (km)	34.1	8.5	12.9	12.0	88.1		
SHIFT TIME (min)	762	162	134	91	415		744
	---	160	132	91	468		
IW DIR (deg)	345/355	315	315	295/275	295	---	298
MOOR DIR (deg)	286	286	286	286	286		
SHIFT DIST (km)	33.1	7.4	10.0	6.2	44.1		76
IW SPEED (m/s)	0.72	0.76	1.24	1.14(1.54)	1.77		1.70
		0.77	1.26	1.14	1.57 (1.67)		
IW WIDTH (km)	---	0.7	1.5	0.9	1.4	---	1.4
			1.6	1.5	1.4		2.5
SOLITON #	---	---	3	3	3	5	3
IW LENGTH (km)	---	1.2	2.4-1.6	4.2-1.6	4.4-2.1	9.7-2.4	4.3-2.8
			7.6-1.8	10.4-2.4	10.5-3.6	7.9-2.5	13.3-5.2
CURRENT (m/s)	0.3	0.5	0.9	0.6	1.2	---	---
	---	0.4	1.2	0.8	1.6	---	---
AMPLITUDE (m)	---	---	(80/90)	(32/63)	(70/95)	---	---

Table 2. SAR AND MOORING DATA COMPARISON on May4-5

SENSOR (ADCP)	S2	S3	S4	S5	S6	S7	S8	SAR
DEPTH (m)	71	85	120	184	275	350	800	---
DISTANCE (km)		15.1	19.0	8.5	12.9	12.0	88.1	
SHIFT TIME (min)		---	420	67	117	84	----	744
		---	---	59	122	78	437	
IW DIR (deg)	0	350	345	325*				283
			285	315*	275	295		280
MOOR DIR (deg)	286	286	286	286	286	286	286	
SHIFT DIST (km)		15.0	19.0	8.0	8.5			
			9.8	6.1	8.5	6.2	38.6	56
IW SPEED (m/s)		---	0.75	2.00*	1.21	1.23	---	----
				(0.77)	(1.18)	(1.72)		
			----	1.72*	1.16	1.32	1.47	1.26
			(1.43*)	(1.10)	(1.63)	(1.72)		
IW WIDTH (km)			0.7	0.8	1.2	0.8	0.8	1.5
SOLITON #	Linear	---	3	2	3	1	1	2
IW LENGTH (km)	0.2	---	1.3-1.0	2.1	1.9-1.5	---	---	2.0
CURRENT (m/s)	---	---	---	0.3	0.3	0.3	---	---
	0.3	---	0.5	0.7	0.6	0.5	---	
AMPLITUDE (m)	---	---	---	---	(16/32)	---	---	---

* Effects of Wave-Wave Interaction

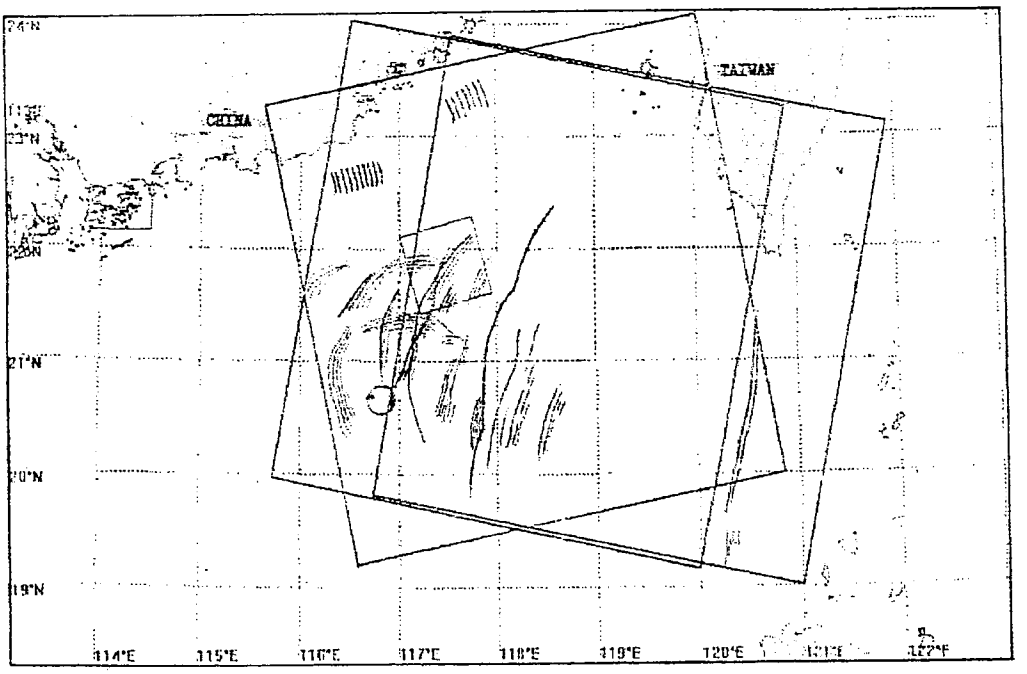

Figure 1. Internal wave distribution map in the ASIAEX area delineated from RADARSAT ScanSAR images collected on May 2, 9, and 18, 2001. The ScanSAR coverage areas are indicated by three large square boxes of 500 km. The small square box is the ASIAEX test area.

Figure 2. RADARSAT ScanSAR image collected northeast of the South China Sea on May 9, 2001 (21:57:34), showing internal wave packets (AB and CD), moorings S5, S7, S8 in white stars, and squall line with rain cells as very bright areas along the front.

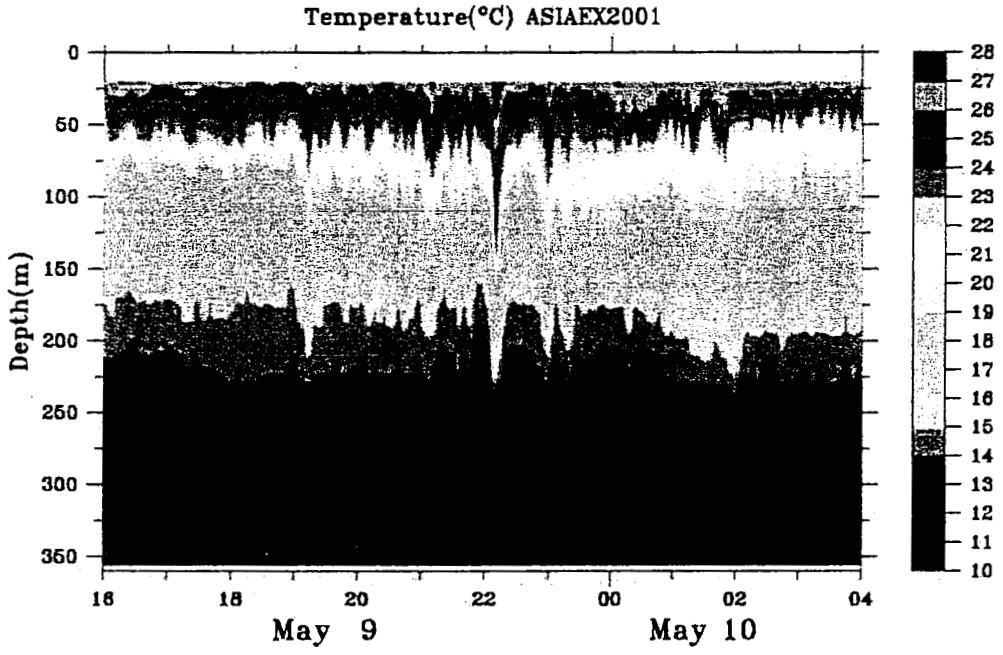

Figure 3. Temperature data from mooring S7 from 16:00 May 9 to 04:00 May 10, 2001. The solitons measured near 22:00 on May 9 corresponds to the solitons observed in SAR image (transect C1-D1) in Figure 2.

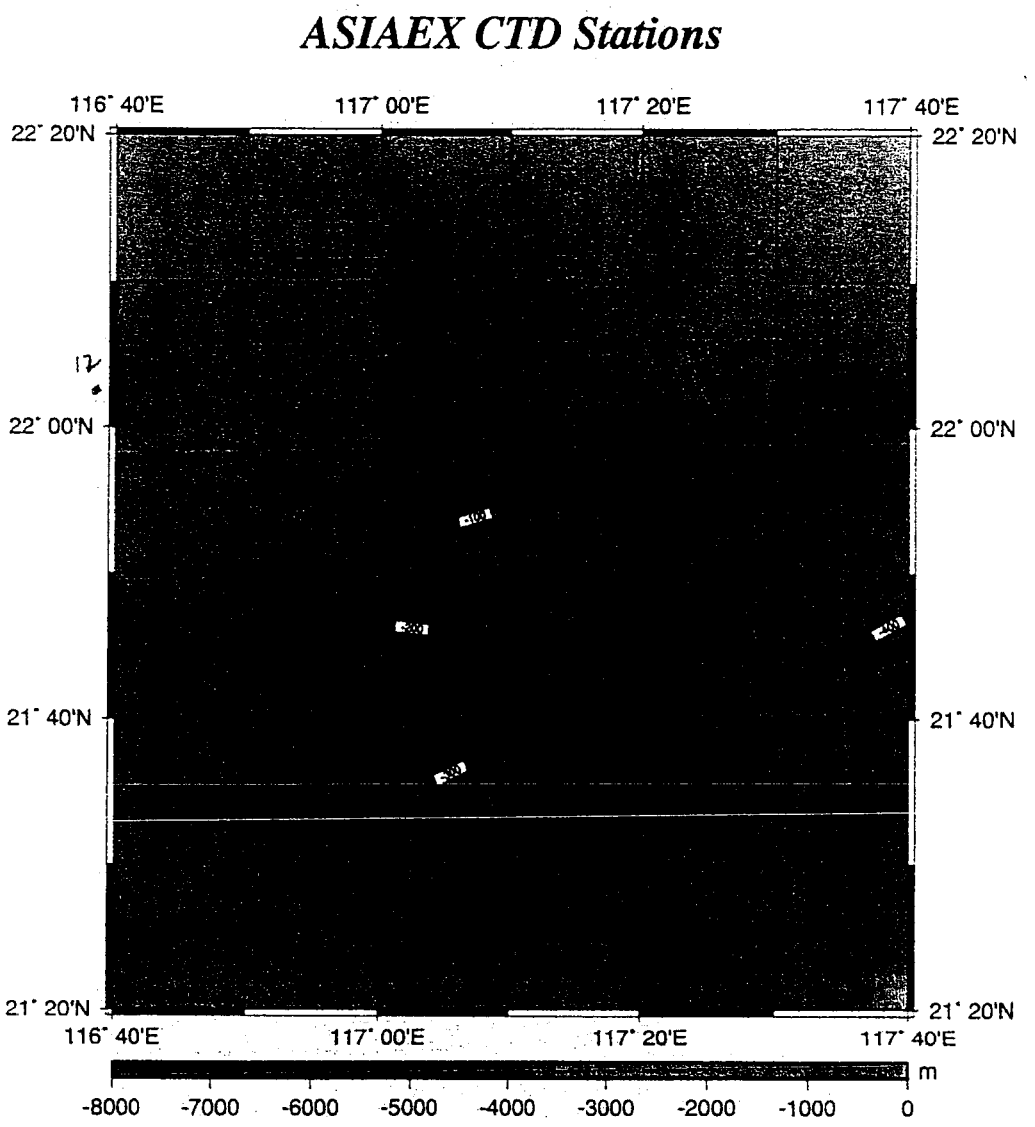

Figure 4. CTD stations during ASIAEX-2001 in the South China Sea.

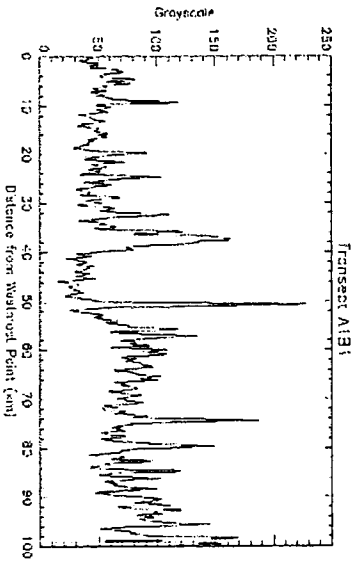
Grayscale
Transect A131
Distance from Westrost Point (km)

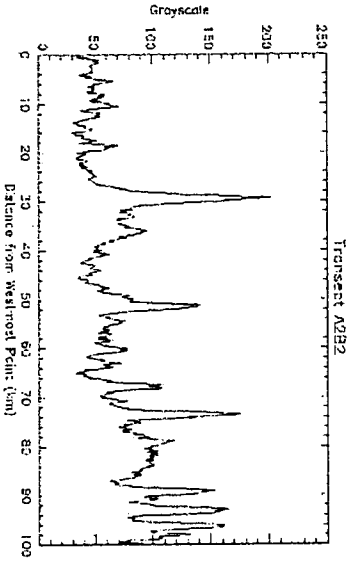
Grayscale
Transect A232
Distance from Westrost Point (km)

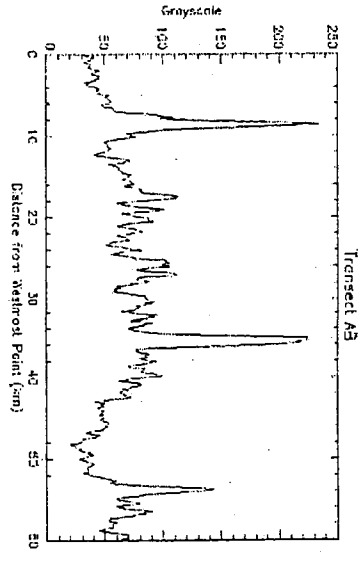
Grayscale
Transect A3
Distance from Westrost Point (km)

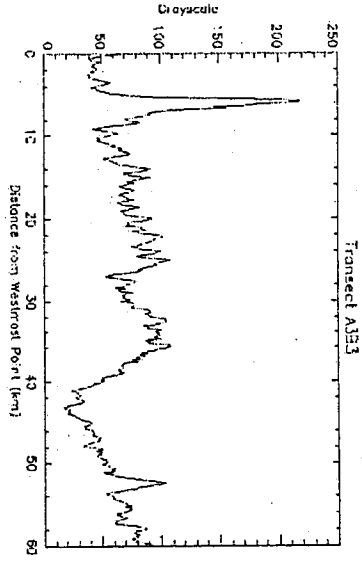
Grayscale
Transect A133
Distance from Westrost Point (km)

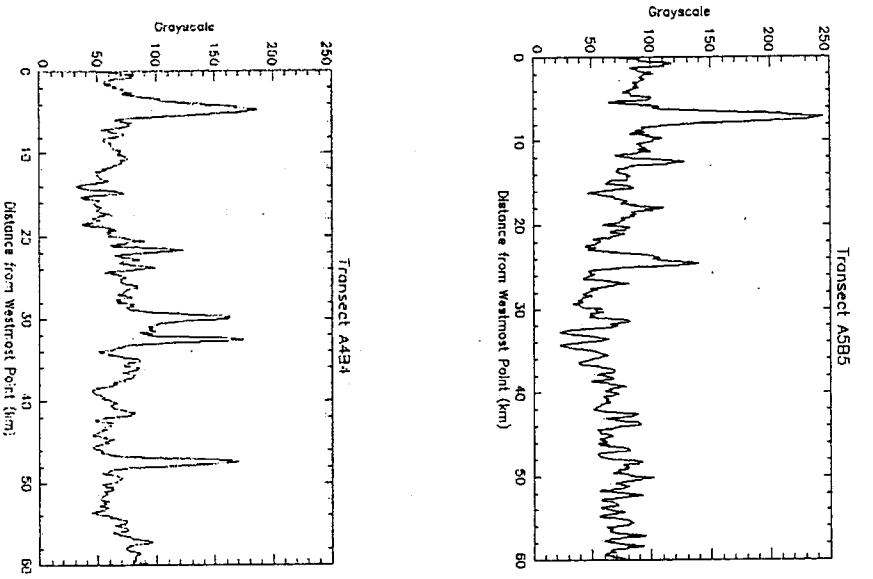

Figure 5. SAR transects across and perpendicular to soliton along (a)A1-B1, (b)A2-B2, (c)AB, (d)A3-B3, (e)A4-B4, and (f)A5-B5 showing the variability of soliton along the wave front of packet in Figure 2.

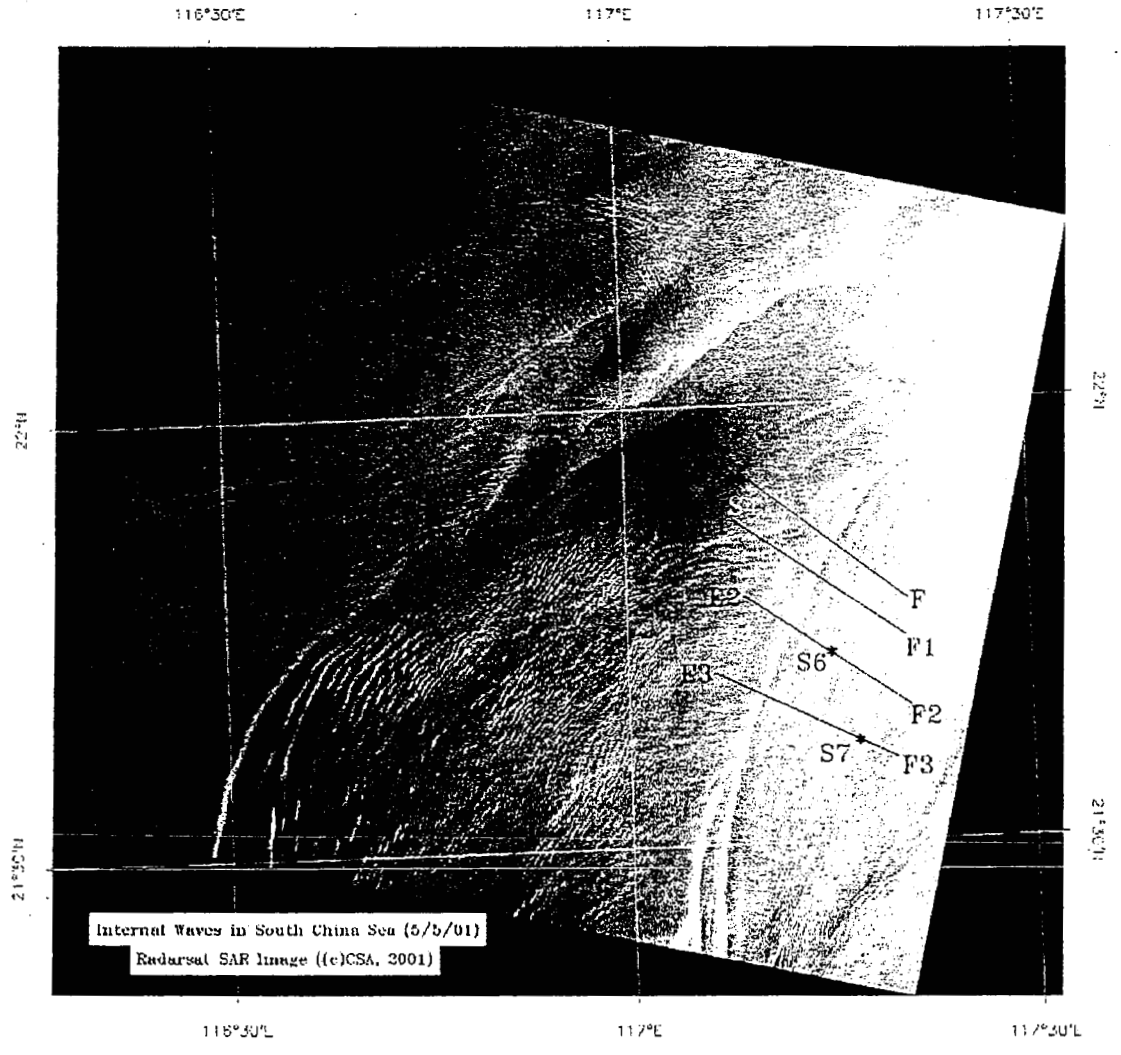

Figure 6. RADARSAT Standard SAR image collected over ASIAEX area on May 5, 2001, showing internal wave packets (EF) and mooring S4, S5, S6, and S7 by stars [16].

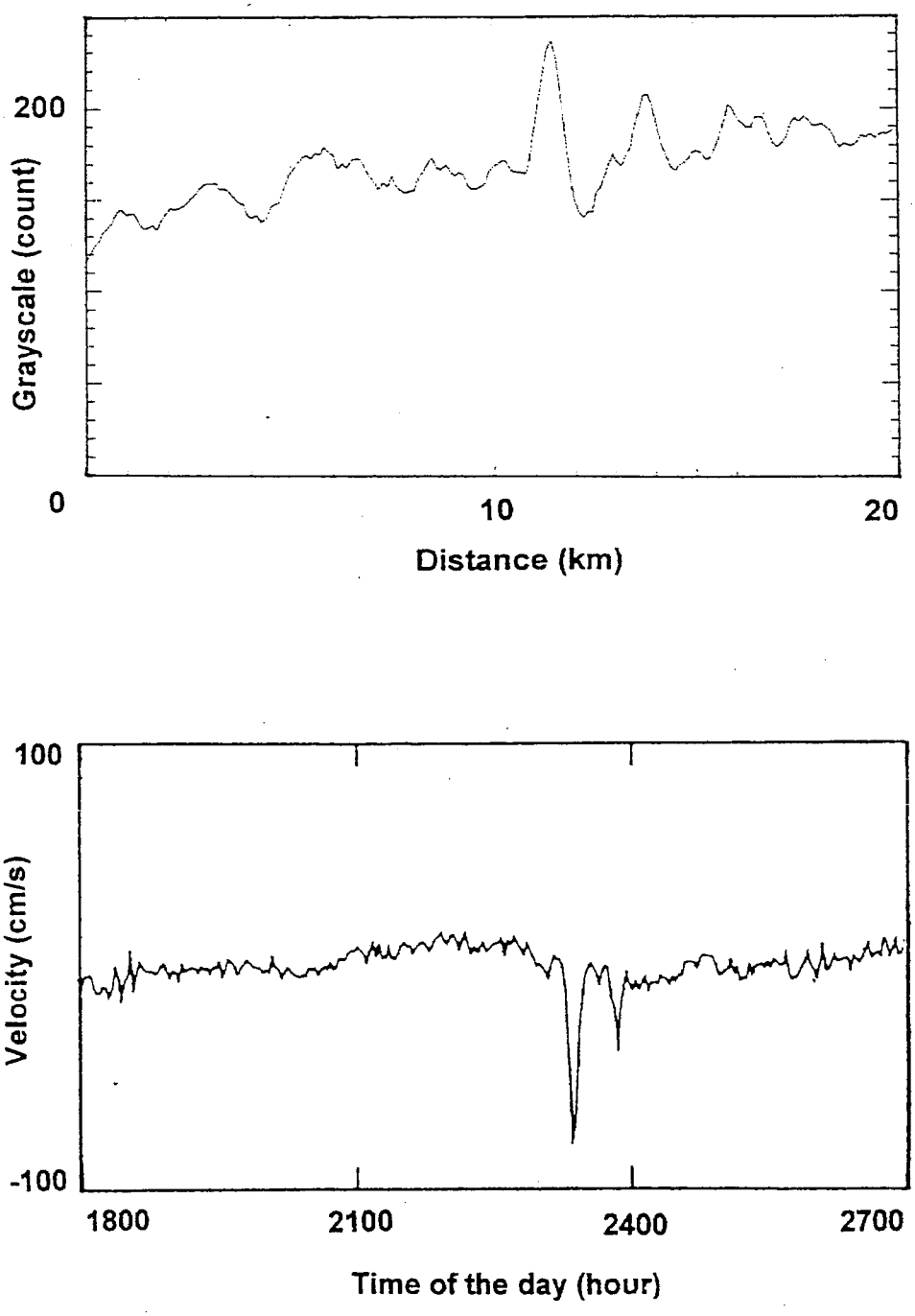

Figure 7. (a) SAR transect across and perpendicular to soliton packet along E1-F1 compared with (b) ADCP current data at mooring S5 on May 5. The wave speed can be estimated based on the distance between S5 and wave front in SAR image (Figure 6).

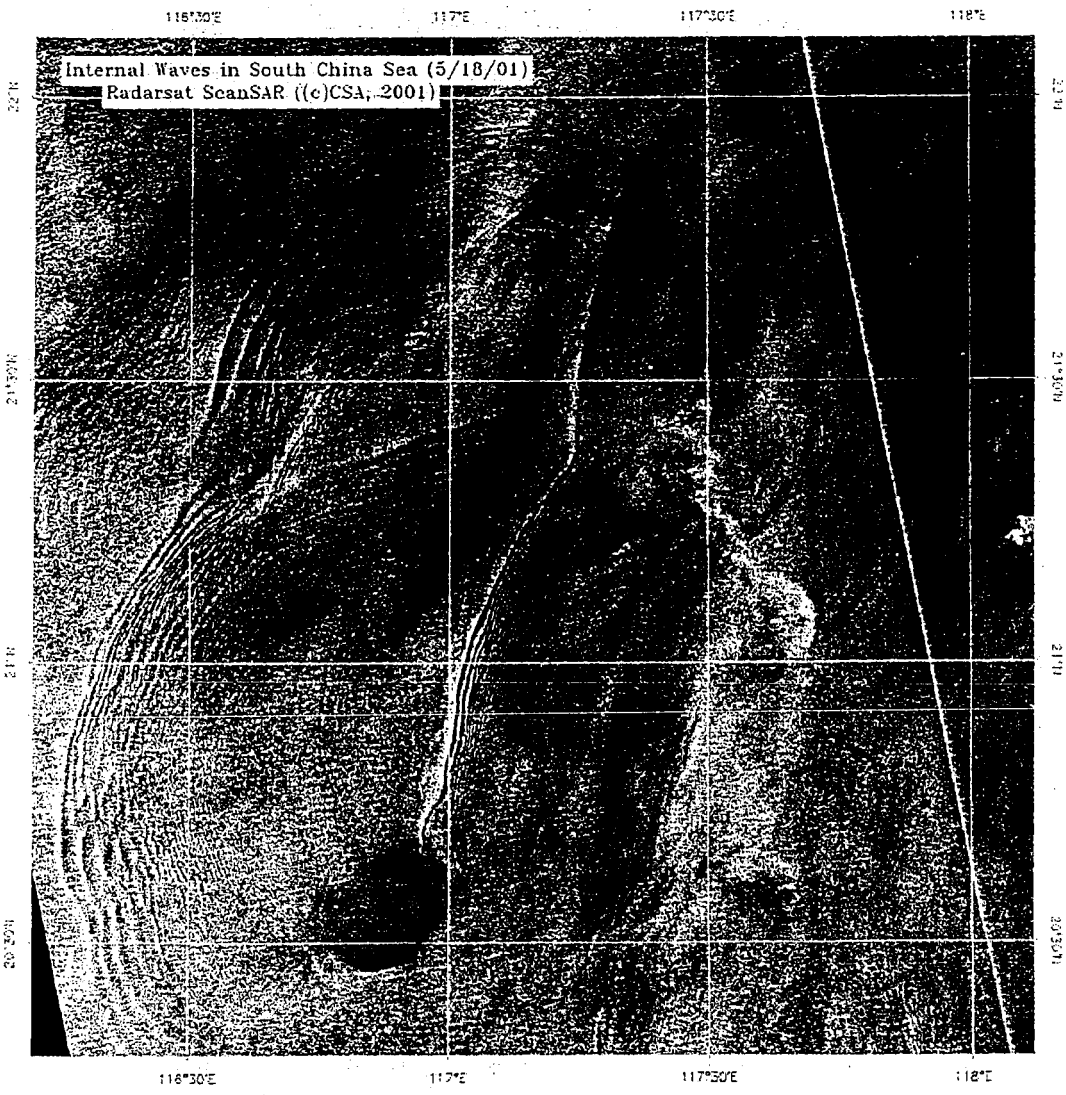

Figure 8. Subscene of RADARSAT ScanSAR image collected over ASIAEX area on May 18, 2001, showing wave-wave interaction of two wave packet system.

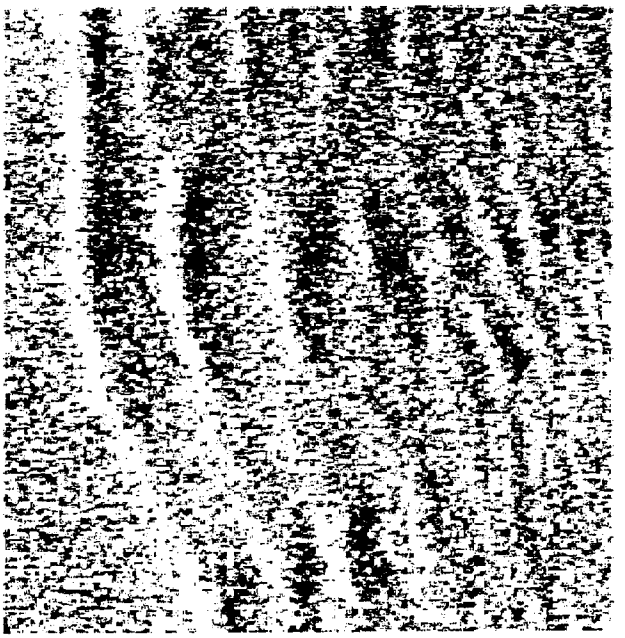

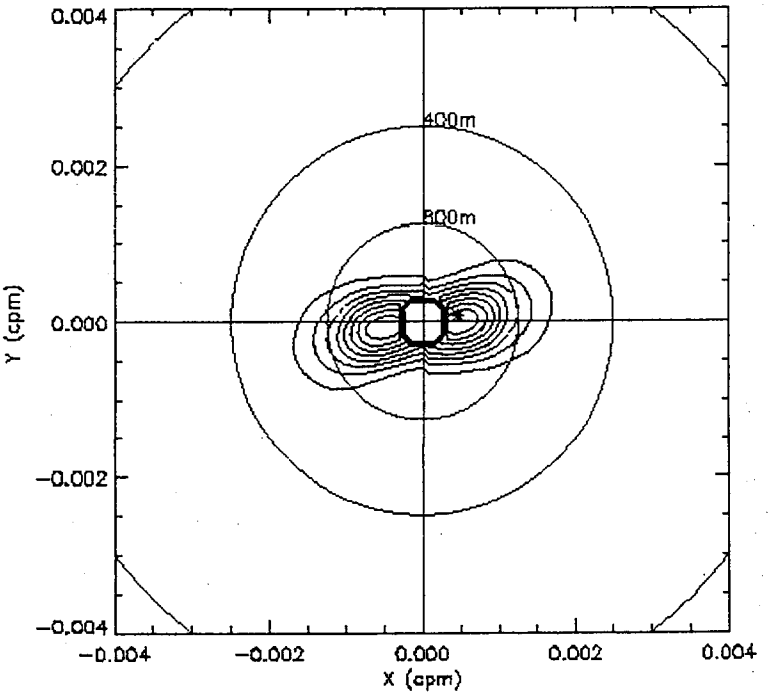
0.004
0.002
0.000
−0.002
−0.004
Y (cpm)
400m
800m
−0.004
−0.002
0.000
0.002
0.004
X (cpm)

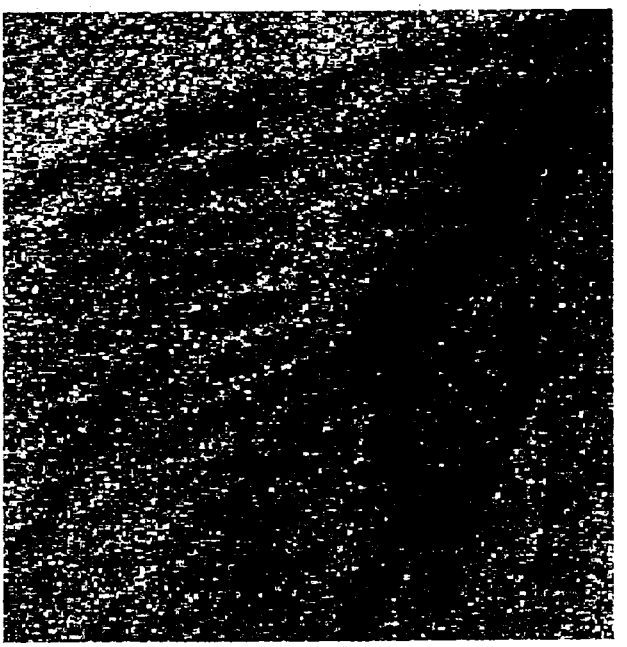

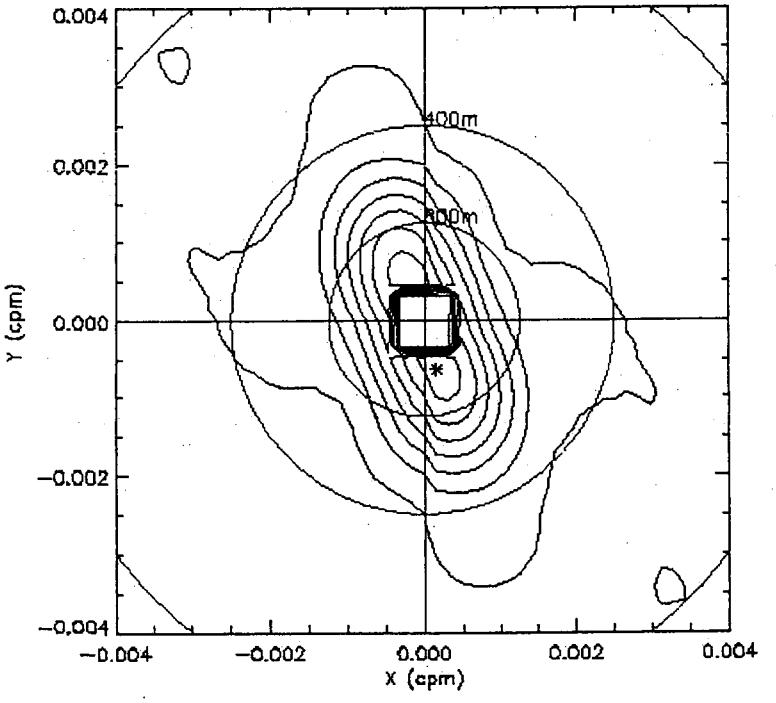
0.004
0.002
0.000
−0.002
−0.004
Y (cpm)
400m
800m
−0.004
−0.002
0.000
0.002
0.004
X (cpm)

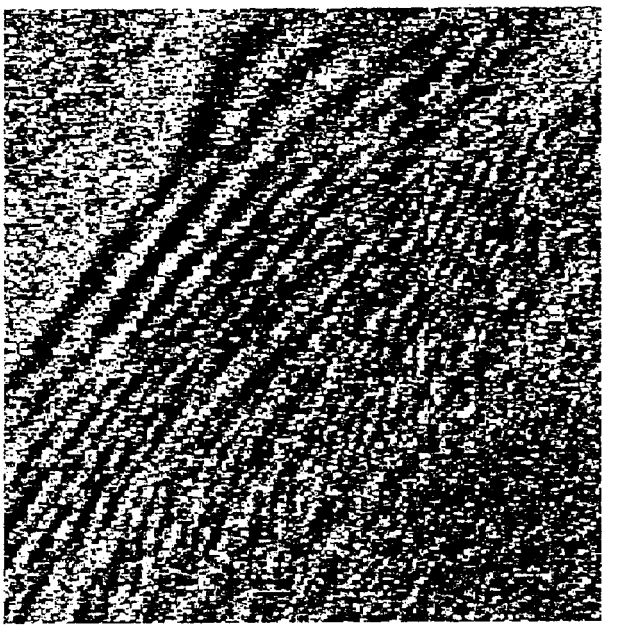

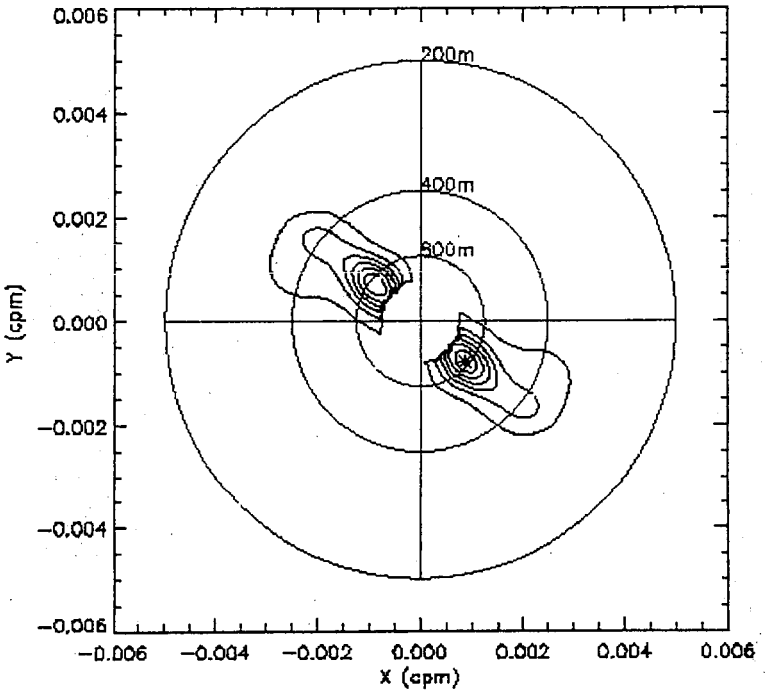

Figure 9. Subscenes of SAR images and two-dimensional wave number spectra of (a)East-West travelling solitons, (b) North-South travelling wave packet, and (c) waves in the interaction zone.

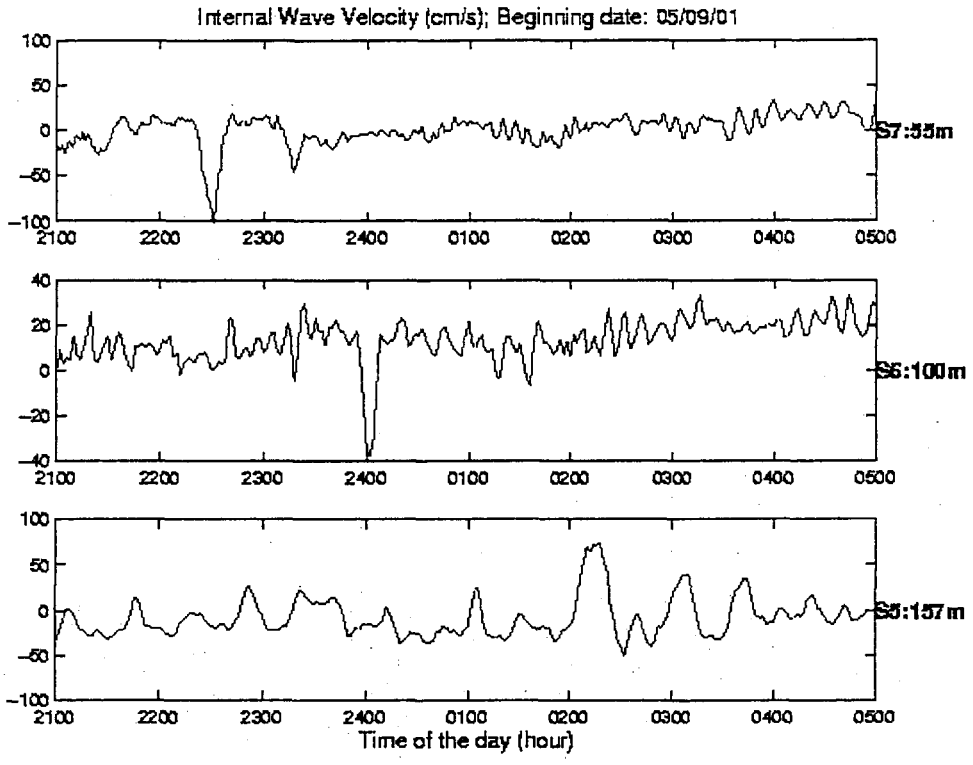

Figure 10. ADCP current time series data from moorings S5, S6, and S7 with soliton packets identified from SAR image (Figure 2) on May 9 to 10, 2001 showing mode-1 internal waves passing through ASIAEX area. The shift/lagging time between moorings can be estimated from the arriving time of each identified packet.

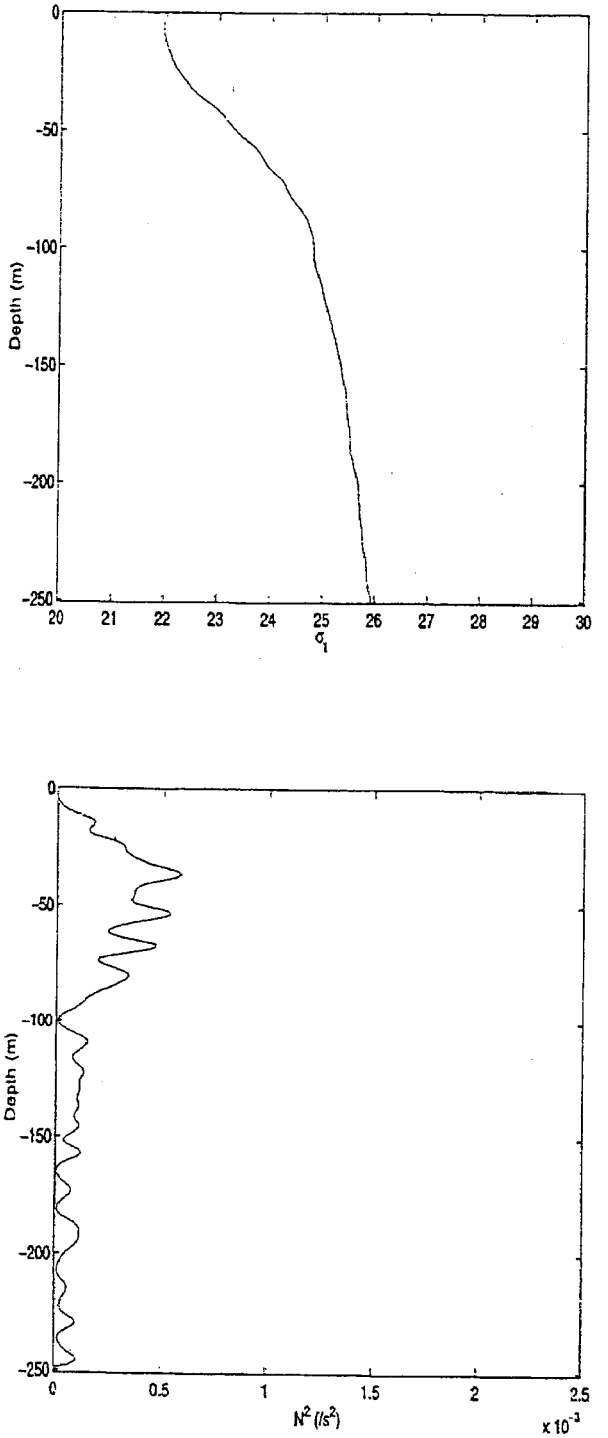

Figure 11. (a) Density and (b) Brunt-Vaisala frequency profiles at mooring S6.

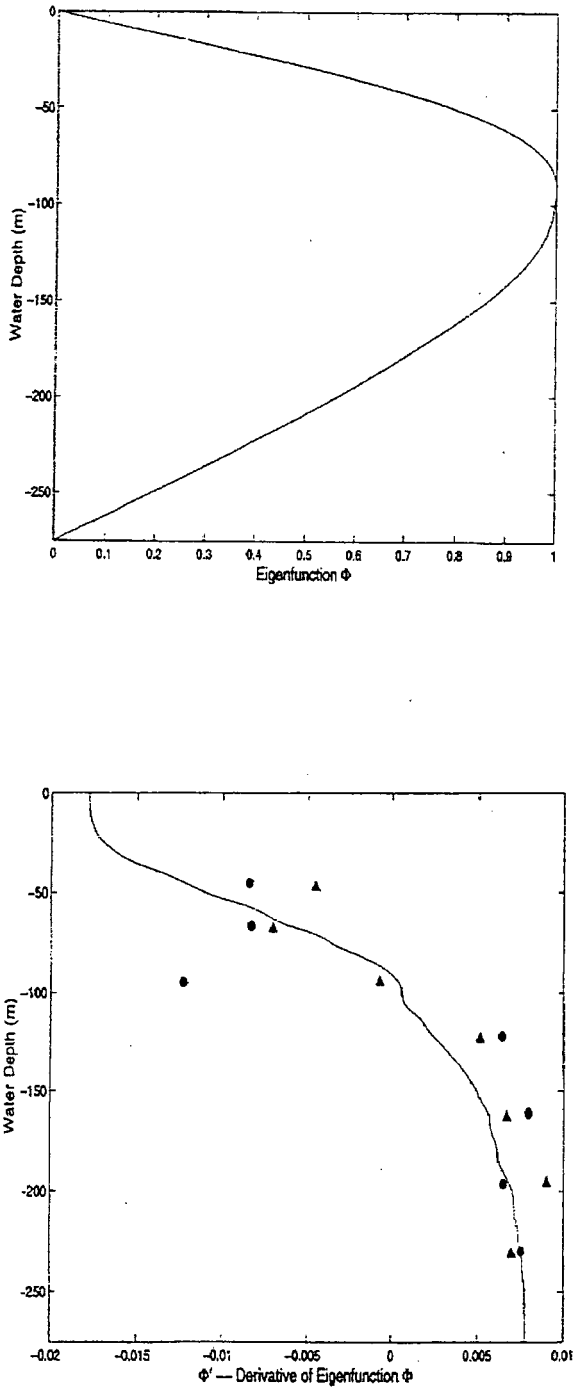

Figure 12. (a) Mode-1 vertical eigenfunction profile, and (b) its derivative for current profile induced by internal waves. The current data indicated by solid circles and triangles are ADCP measurements at mooring S6 on May 9 for two different wave packets.

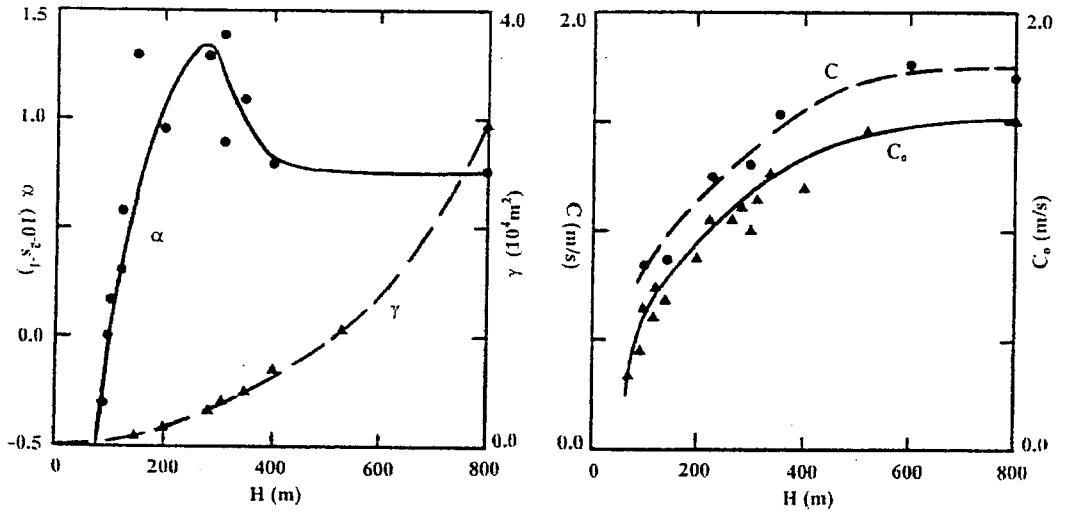

Figure 13. Internal wave environmental parameters as a function of depth based on CTD data.

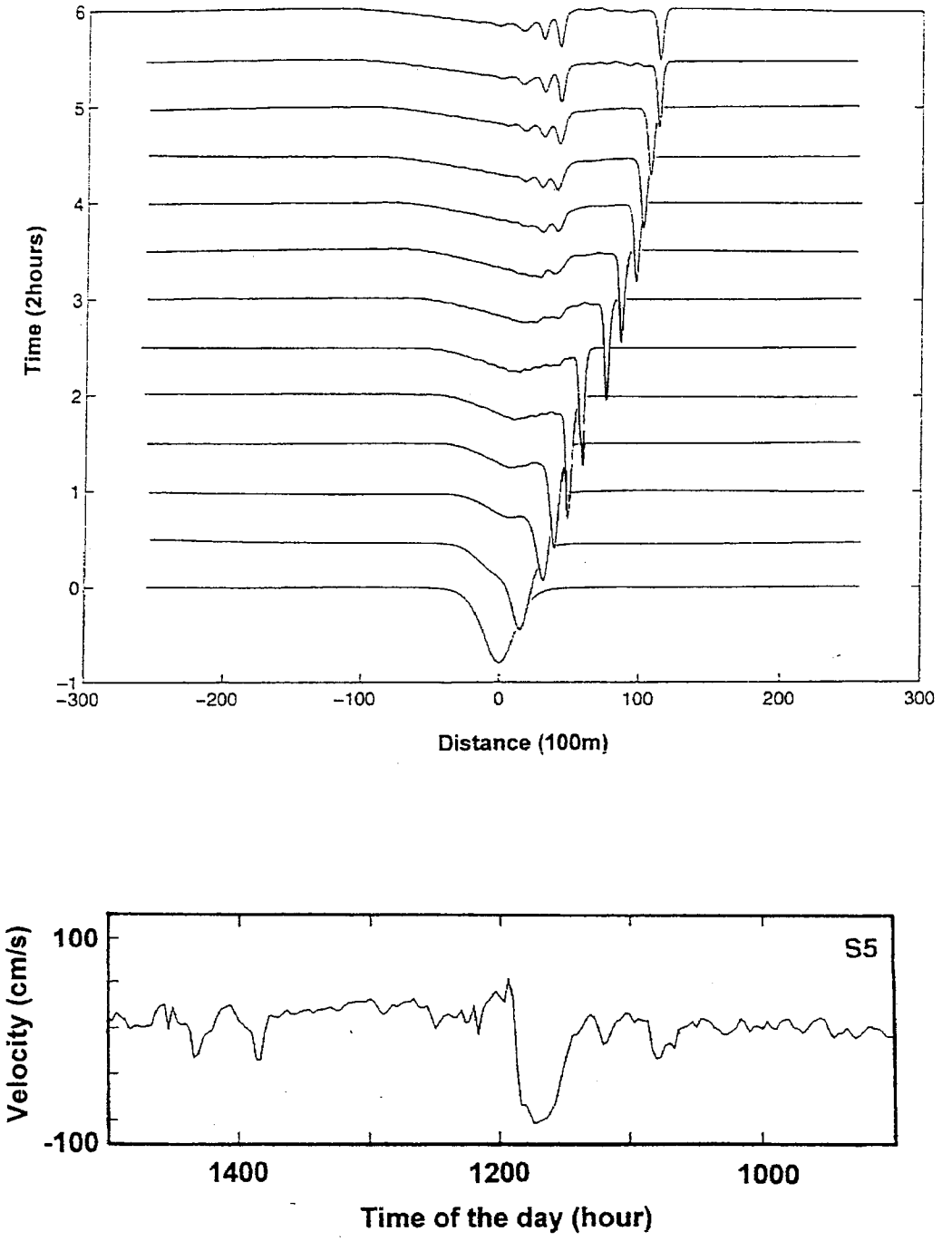

Figure 14. (a) Numerical simulation of a nonlinear soliton propagating from SAR observation in deep water evolved into three solitons in a packet at mooring S5 on shelf and compared with (b) S5 ADCP current measurement.

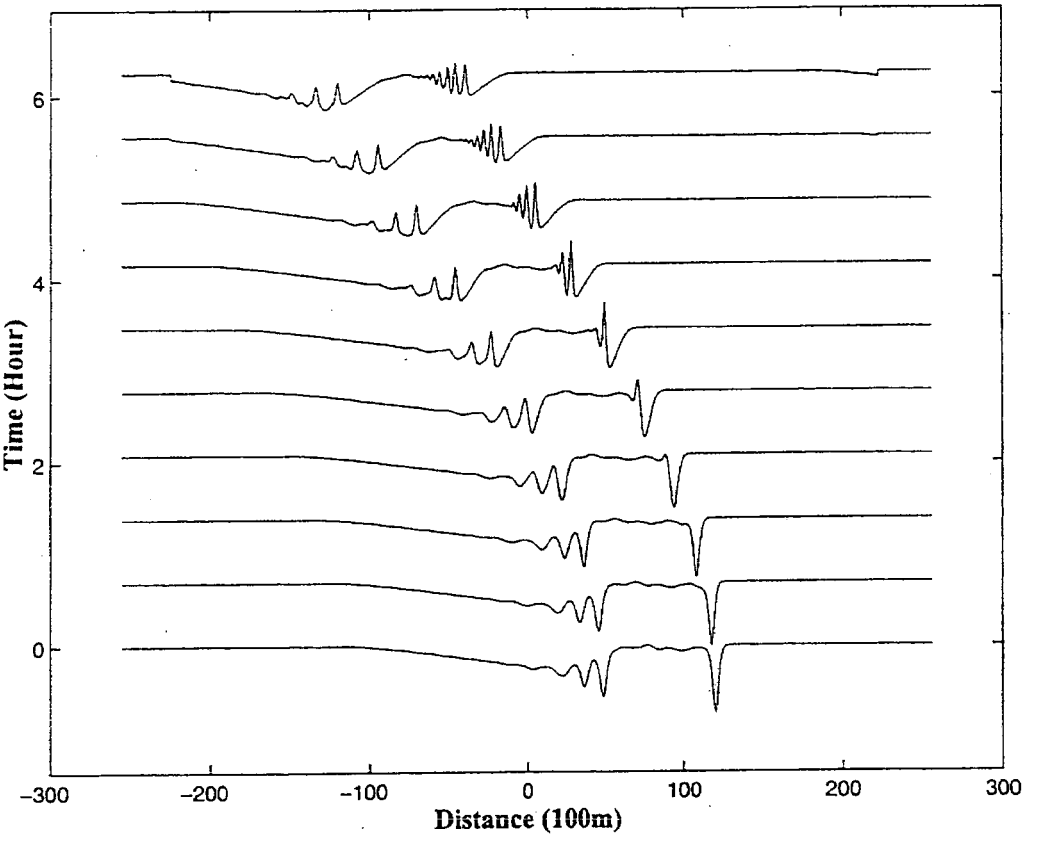
Time (Hour)
6
4
2
0
−300
−200
−100
0
100
200
300
Distance (100m)

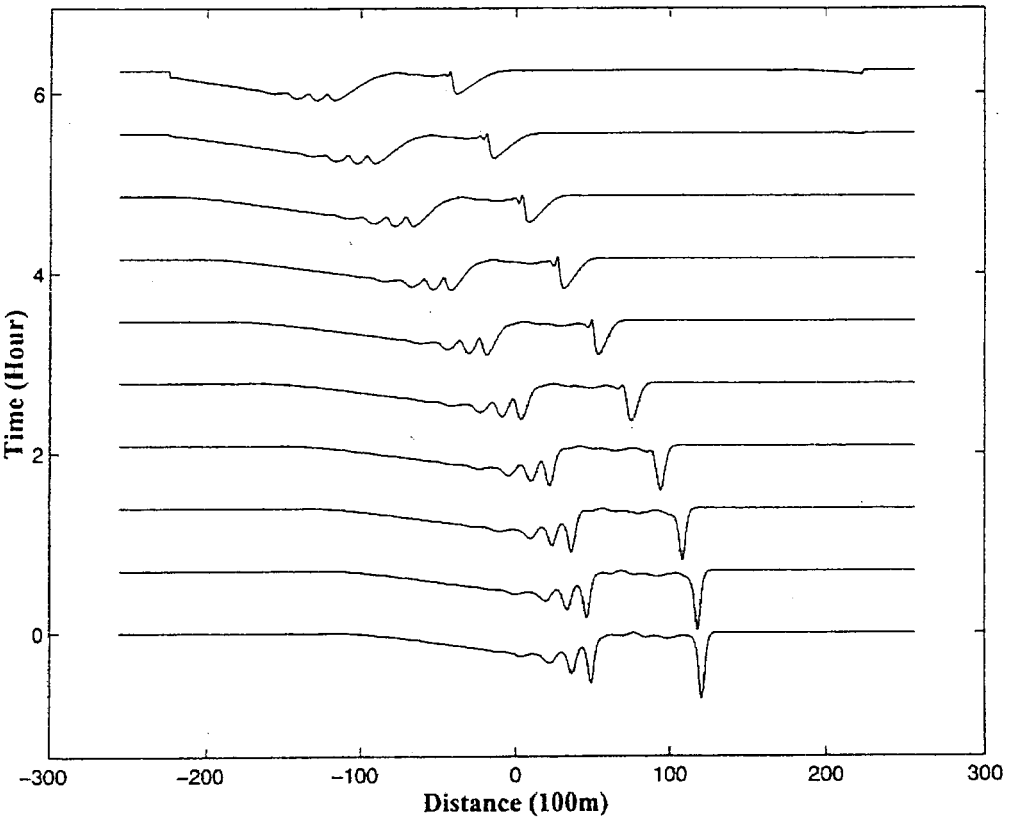

Figure 15. Numerical calculation of the internal soliton packet propagating from mooring S5 (Figure 10) to mooring S3 in shallow water for (a) decreasing dissipation, and (b) constant dissipation (ε = 6 m^2/s). The change of polarization from depression waves to elevation waves across the critical depth has been demonstrated in the first simulation.

Model-Data Assimilation of Internal Waves during ASIAEX-2001

by A. K. Liu, Y. Zhao, T. Y. Tang, and S. R. Ramp

Popular Summary:

In recent Asian Seas International Acoustics Experiment (ASIAEX), extensive moorings have been deployed around the continental shelf break area in the northeast of South China Sea in May 2001. Simultaneous RADARSAT SAR images have been collected during the field test to integrate with the in-situ measurements from moorings, ship-board sensors, and CTD casts. During ASIAEX in May 2001, many large internal waves were observed at the test area and were the major oceanic features for acoustic volume interaction. Based on the internal wave distribution maps compiled from satellite data, the wave crest can be as long as 200 km with amplitude of 100 m. Environmental parameters have been calculated based on extensive CTD casts data near the ASIAEX area. Nonlinear internal wave models have been applied to integrate and assimilate both SAR and mooring data. The numerical simulations produce the wave evolution on the continental shelf and compared reasonably well with the mooring measurements at the downstream station.

Significant Findings:

The shoaling, turning, and dissipation of large internal waves on the shelf break, elevation solitons, and wave-wave interaction have been studied and are very important issues for ocean mixing processes and acoustic propagation. Besides it provides synoptic information, satellite imagery is very useful for tracking the internal waves, and locating surface fronts and mesoscale features. The internal wave effects on acoustic volume scattering and modal coupling have been implicated and found very significant.